Chapter

Why Al-B_4C Metal Matrix Composites? A Review

Mohamed F. Ibrahim, Hany R. Ammar, Agnes M. Samuel, Mahmoud S. Soliman, Victor Songmene and Fawzy H. Samuel

Abstract

The Al-B_4C metal matrix composite (MMC) is characterized by its ability to absorb neutrons which makes it the most suitable shielding material for nuclear reactors. The present work was performed on two series of Al-B_4C metal matrix composites made using a powder injection apparatus. In one series, commercially pure aluminum (A5) served as the matrix. For the second set, 6063 alloy was used. In all cases the volume fraction of B_4C reinforcement particles (grit size 400 mesh, purity 99.5%) was approximately 15%. The volume fraction of the injected B_4C particles was determined using a computer driven image analyzer. Measured amounts of Ti, Zr, and Ti + Zr, were added to the molten composites of both series. Microstructural characterization was carried out employing a field emission scanning electron microscope operating at 20 kV and equipped with an electron dispersive x-ray spectroscopic system (EDS). The same technique was applied to characterize the fracture behavior of the tested composites. Mechanical properties of these composites were investigated using impact testing, and ambient and high temperature tensile testing methods. Almost 1000 impact and tensile samples were tested following different heat treatments. The obtained results from these investigations are reported in this Chapter.

Keywords: MMC, precipitation hardening, FESEM, tensile testing, impact testing, microstructural characterization

1. Introduction

The Al-B_4C metal matrix composite (MMC) is characterized by its high thermal conductivity and its ability to absorb neutrons which makes it a suitable shielding material [1]. Increasing the concentration of B_4C (>30%) increases the composite strength as well as its neutron absorption capacity. Roy et al. [2] suggested the use of 7xxx alloys as base material for the MMC due to its low density and its hardening ability caused by heat treatment which would contribute to the strength of the MMC. The use of 2124 Al alloy composites reinforced with B_4C particulates has been proposed by Öksüz and Oskay [3]. The authors claim that the volumetric wear rates of the 2124 Al alloy and its composites are increased with increase in the applied load. Singla et al. [4] proposed the use of molten technique for the production of Al-B_4C MMC. The authors studied an MMC made of Al-7075 alloy as the matrix and B_4C 32 μm particulate as the reinforcement agent. Mohan and Kennedy [5] investigated the machinability of Al-(7 and 14) wt.% Si alloys reinforced with B_4C. The MMCs were developed using the stir casting technique. Their results show that the composite reinforced with B_4C with a particle size of 100 nanometers has better mechanical properties and wear behavior compared to those reinforced with 24-micron or 6-micron sized particulates. Vaidya et al. [6] found that the strength of B_4C particle reinforced Al 6061 composite was significantly greater than the unreinforced alloy.

Drilling experiments were conducted by Kumar et al. [7] on 6061 alloy-15%B_4C (220 μm particulate diameter) using a vertical machine with High Speed Steel drills of 6 mm, 9 mm and 12 mm diameter under dry drilling conditions. It was found that speed, design of the experiment and drill diameter have a marked influence on the Over-Cut (half the difference of the diameter of the hole produced to the tool diameter). Topcu [8] and Manjunatha et al. [9] used the powder atomization technique to produce Al-5% B_4C and Al-15%B_4C MMCs. The authors reported that the wear resistance increased in proportion to the amount of the boron carbide reinforced. Tribo-surface characteristics of two aluminum metal matrix composites (Al-MMC) of compositions Al–13 vol%B_4C and Al–13 vol%SiC sliding against a commercial phenolic brake pad under dry conditions were investigated by Shorowordi et al. [10–12]. The friction coefficient was found to decrease slightly at high contact pressure.

The wear rate and friction coefficient of Al–B_4C was lower than that of Al–SiC. Several studies on friction behavior involving Al-MMC friction against ferrous materials revealed that during sliding, a layer, termed as mechanically mixed layer (MML), was formed on the worn surface of the Al-MMC [13–17]. Such layer, however, was not found to form on unreinforced aluminum. Several researchers [18–22] studied the production of Al-11%B_4C using stir melt technique. The 6061 alloy was the matrix to which B_4C particles were added. Prior to addition, the B_4C particles were preheated along with K_2TiF_6 halide salt. The resulting composite was found to have improved mechanical properties compared to the base alloy. Uthayakumar et al. [23] performed a study on the wear performance of Al–5%SiC–5%B_4C hybrid composites under dry sliding conditions using a pin on disc tribometer method. The main conclusion was that the hybrid composites can retain the wear resistance properties up to 60 N load and sliding speed ranges of 1–4 m/s.

Comparison of microstructural and mechanical properties of Al–10 vol% TiC, Al–10 vol% B_4C and Al–5 vol% TiC–5 vol% B_4C composites prepared by casting techniques was made by Mazaheri et al. [24]. The results show that the wear behavior of Al-B_4C MMC is the best among the three composites studied. The wettability of B_4C particulates was investigated by Toptan et al. [25]. They found that addition of Ti leads to formation of thin layers (80–180 nm in thickness) of Ti-C and Ti-B around the B_4C particulates which would solve the wettability issue. Similar observation on titanium as one of the reactive metals that can be used to increase wettability in Al-B_4C system was reported by other researchers [26–31]. According to Wang et al. [32] and Yang et al. [33], the stress distribution within a particle-reinforced composite subjected to external loading is non-uniform. Nanostructured Al–B_4C composite sheets were processed by accumulative roll bonding (ARB), and the effect of the number of ARB cycles on the distribution of the B_4C particles in the Al matrix was evaluated by Yazdani and Salahinejad [34] who noted an improvement in the reinforcement distribution by increasing the ARB cycles.

The present chapter summarizes the work that was carried out by the present authors using two types of Al-B_4C composites: (i) a mechanically alloyed composite supplied by Ceradyne Canada ULC, a 3 M Company, Chicoutimi, Québec, Canada, and (ii) an in-house made composite using powder injection at the Université du Québec a Chicoutimi [35–44].

DOI: http://dx.doi.org/10.5772/intechopen.95772

2. Experimental procedure

2.1 Composite preparation

Reinforcement powder (grit size 400 and 95.4% purity) additions of 15 vol. % were made using a powder injection apparatus (**Figure 1**). The B_4C particulate was injected into molten Al. Fe, Ti and Zr additions were introduced into the molten bath, using Al-25%Fe, Al-10% Ti and Al-15% Zr master alloys, respectively, whereas Mg and Si were added as pure elements. Chemical compositions of the investigated composites are listed in **Table 1**. A general view of the powder injection set-up showing a schematic of the injection system is shown in **Figure 1**. It consists of the following components:

i. a fluidizer tube

ii. a carrier tube and a quartz nozzle

iii. resistance heating coils

iv. an adjustable two-dimensional movable stand

v. a melting unit with resistance heating

vi. an impeller (stirrer) with adjustable rotation speed

vii. flow diversion baffles.

In order to ensure uniform distribution of the B_4C particulates, the molten composite melt was stirred vigorously (300 rpm) at 730 ± 5°C. Thereafter, the molten composite was poured in two different metallic molds preheated at 450°C, as shown in **Figure 2**: an L-shaped mold (3.5x 3.8 x 30.5 cm) which was used for microstructure characterization, and a book-type mold (4 x 17 x 34 cm). In order to determine

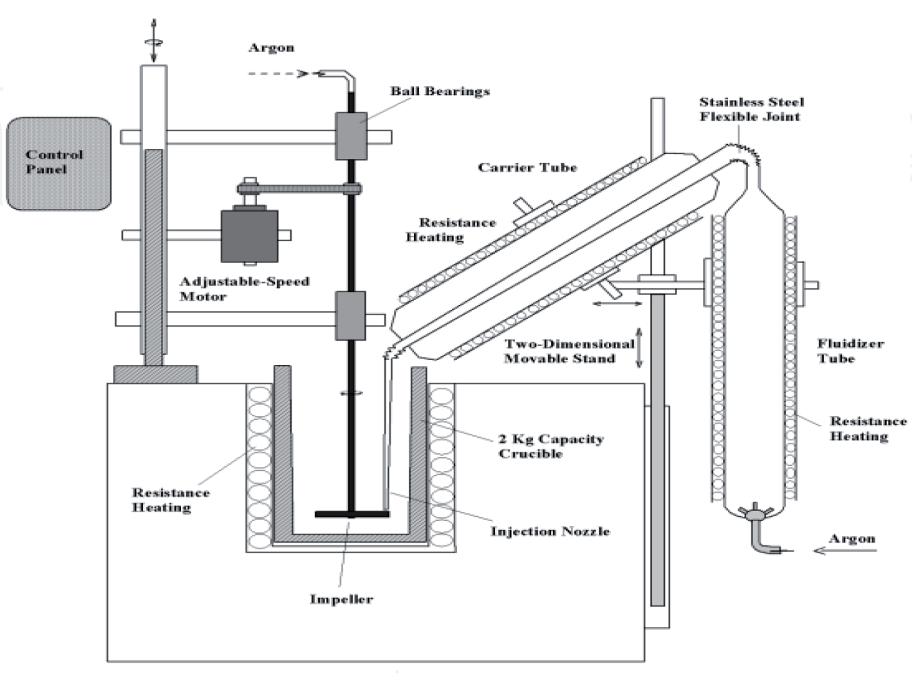

Figure 1.
A schematic diagram of the powder injector used in the present work.

Alloy Code	Composition (Ti, Zr, Sc in wt%)
1A	Al-15v/oB4C
2A	Al-15v/oB4C + 0.45%Ti
3A	Al-15v/oB4C + 0.45%Ti + 0.25%Zr
4A	Al-15v/oB4C + 0.45%Ti + 0.15%Sc
5A	Al-15v/oB4C + 0.45%Ti + 0.15%Sc + 0.25%Zr
1B	6063-15v/oB4C
2B	6063-15v/oB4C + 0.45%Ti
3B	6063-15v/oB4C + 0.45%Ti + 0.25%Zr
4B	6063-15v/oB4C + 0.45%Ti + 0.15%Sc
5B	6063-15v/oB4C + 0.45%Ti + 0.15%Sc + 0.25%Zr

Table 1.
Codes and compositions of the MMCs used in this study.

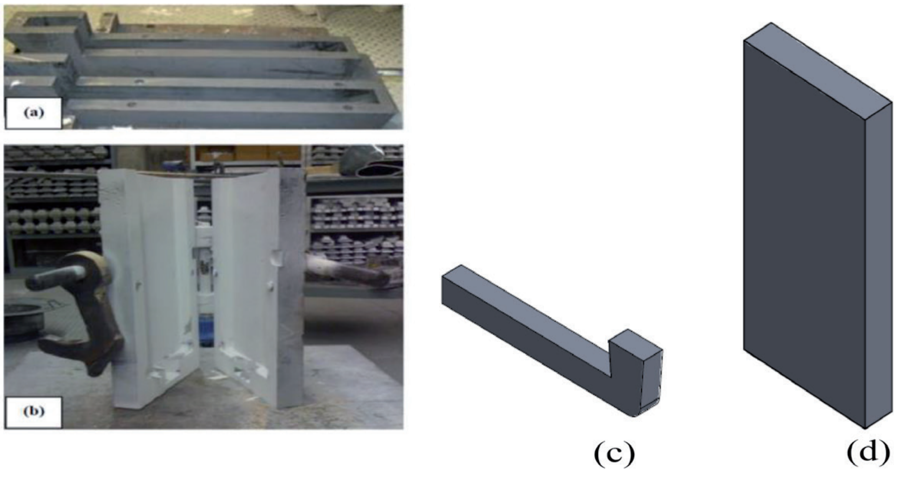

Figure 2.
(a) L-shaped mold, (b) book-type mold, (c) L-shaped casting, (d) book-mold casting.

the solidification rate obtained from each mold, trials were made using Al-7%Si. **Figure 3** depicts the dendrite arm spacing (DAS) and grain size corresponding to each mold. The castings made using the book-mold were hot rolled into slabs of 1-3 mm thickness, depending on the type of test carried out.

2.2 Microstructural investigation

Samples for microstructural characterization were prepared from the L-shaped mold casting in the as cast condition using 5A composite. The volume fraction and average size of the B_4C particles was measured using Clemex image analyzer. Fracture surfaces were examined of samples sectioned from both tensile- and impact tested bars. The samples were examined using Hitachi S-7000 and Hitachi SU-8000 FE-SEM microscopes equipped with EDS facilities at McGill University, Montreal.

2.3 Mechanical testing

Charpy impact testing was carried out on un-notched test specimens (10x 10 x 55 mm). The samples were sectioned from the L-shaped mold castings and heat treated in an electrical air forced furnace. An instrumented Charpy impact testing machine, equipped with a data acquisition unit was employed to measure the load, total absorbed energy (E_t) to fracture. The mean values of 6 impact-tested samples for each composite/condition were reported.

Slabs (25x 20x 400 mm) were prepared from the book mold castings. Prior to rolling using a four cylinder mill, the slabs were annealed at 500°C for 16 h. The last two passes were carried out at room temperature to straighten the rolled slabs (sheets) – see **Figure 4**. **Figure 5** shows the dimensions of samples prepared from

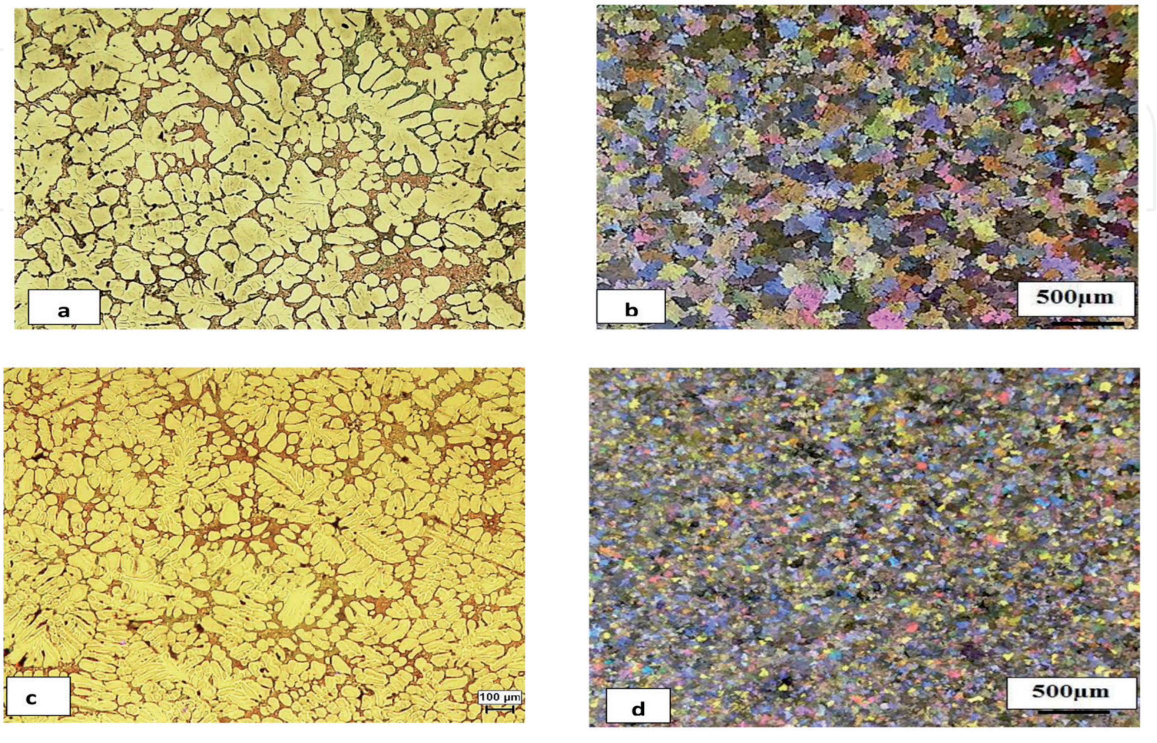

Figure 3.
(a, c) Optical micrographs of Al-7%Si alloy for (a) block casting, 60 µm; (c) L-shaped casting, 30 µm; (b, d) Macrographs showing grain size in (b) block casting; (d) L-shaped casting.

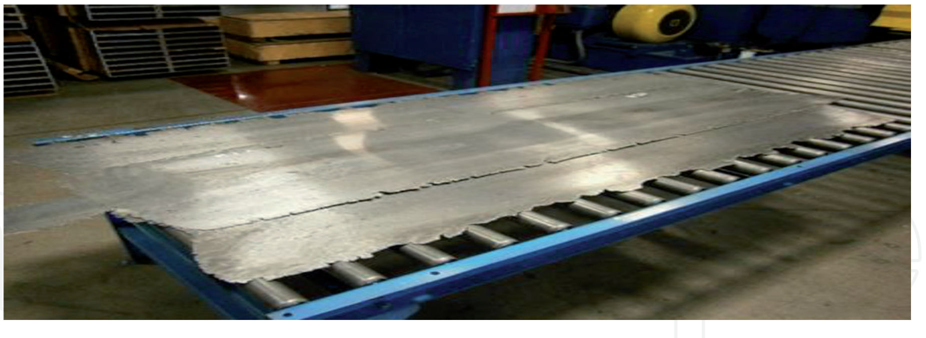

Figure 4.
Hot rolled sheets.

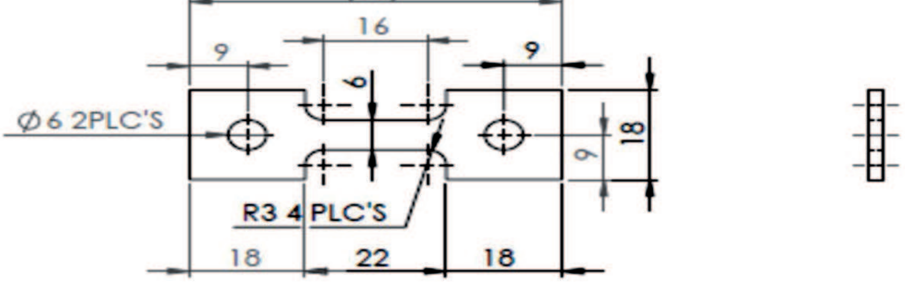

Figure 5.
Typical sample for room and high temperature tensile testing (dimensions are in mm).

the rolled sheets and used for room and high temperature tensile testing. Tensile samples (matrix is aluminum) were solutionised at 620°C for 24 h. In spite of the fact that pure aluminum normally is not heat treatable, it could benefit from the precipitation of Zr-rich particles during aging. The 6063/B_4C/15p composite samples were solutionized at 540°C to minimize surface oxidation (MgO). After solution heat treatment, the tensile bars were quenched in warm water (60° C), followed by aging for 10 h at 200, 300 and 400° C, and then air cooling. Room temperature testing was carried out using an MTS Servohydraulic mechanical testing machine at a strain rate of 4 x 10^{-4}/s.

High temperature testing was done at strain rate of 5 x 10^{-4}/s in a temperature range 25–500°C. In all cases, tensile properties were measured: ultimate tensile strength (UTS), the 0.2% offset yield strength (YS) and percentage elongation (%El). For each working condition, at least five specimens were tested and mean values were reported (SD ±5%). Microstructure and fracture behavior of selected samples were examined using optical microscopy and Field Emission Scanning Electron Microscopy (FESEM) techniques.

3. Results and discussion

3.1 Microstructural characterization (as cast condition)

The main function of the addition of Zr and Ti, is to protect the B_4C particles from reacting with the molten Al [45–48]. **Figure 6(a)** depicts the microstructure of a specimen sectioned from the L-shaped castings, revealing a uniform distribution of B_4C particles throughout the matrix. From such micrographs, the volume fraction of B_4C particles was determined (~15 vol.%). According to the Al–Ti binary diagram [49], at 730°C an amount of 0.5 wt-%Ti could be added to the molten composite. From the reported findings of Tahiri et al. [50–54] it was reported that increasing the concentration of Ti in the molten alloy above 0.5 wt.% will increase the temperature of the molten alloy. As a result, fluidity of the composite will be markedly reduced caused by the segregation of B_4C particles as exhibited in **Figure 6(b)**.

FESEM examination of 5A composite treated with Ti revealed that in addition to B_4C particles, possible precipitation of several intermetallics mainly, TiB_2, TiC and traces of $AlB_{24}C_4$, Al_4C_3, Al_3BC and AlB_{12}, along with the primary intermetallic phases TiAl, Ti_3Al and $TiAl_3$ could also occur. It is expected that the formation of these phases in layers would lead to an improvement in the adhesion between the matrix and the B_4C reinforcement [21–23]. **Figure 7** displays electron micrographs of alloy B,

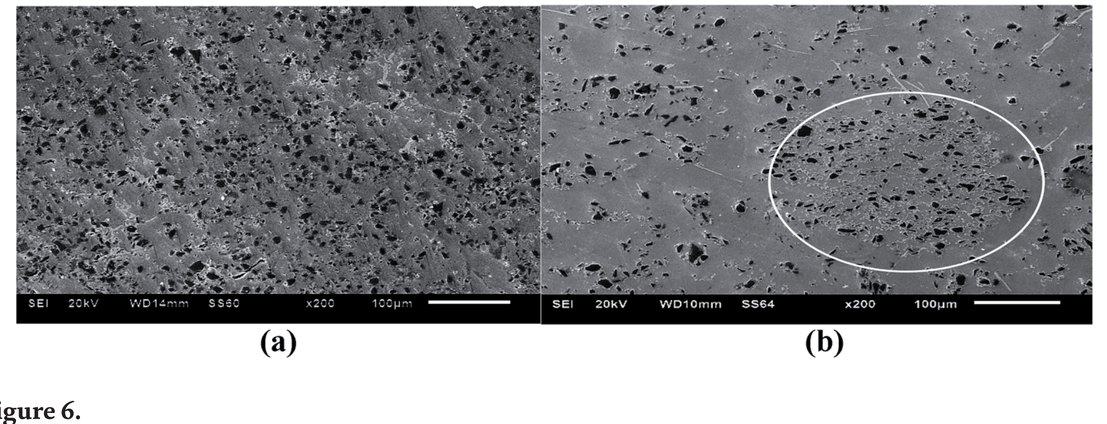

Figure 6.
Secondary electron micrographs showing: (a) a uniform distribution of B_4C in matrix of base alloy using in-house powder injecting technique, (b) segregation of B_4C (white circle).

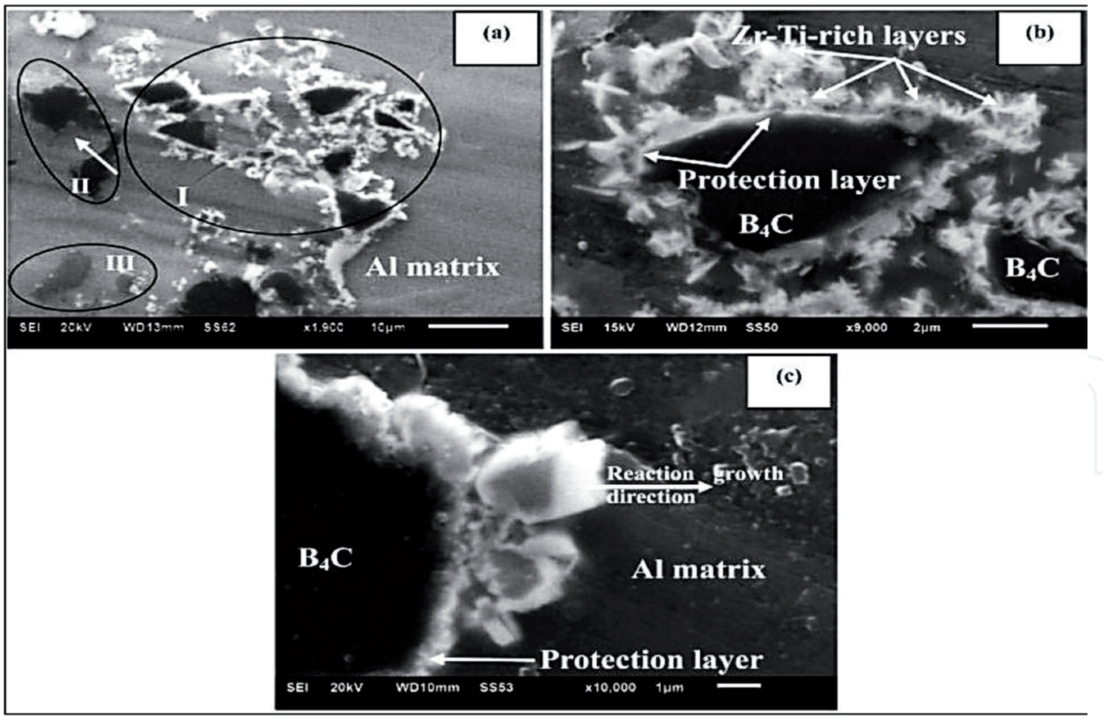

Figure 7.
SE images from composite B showing (a) regular B$_4$C particles protected by layers of Zr–Ti rich particles, (II) irregular forms of B$_4$C showing partial reaction with matrix forming AlBC compound; (b) B$_4$C particle surrounded by two layers of Zr–Ti rich particles; and (c) B$_4$C particle showing progress of cumulative reaction towards matrix.

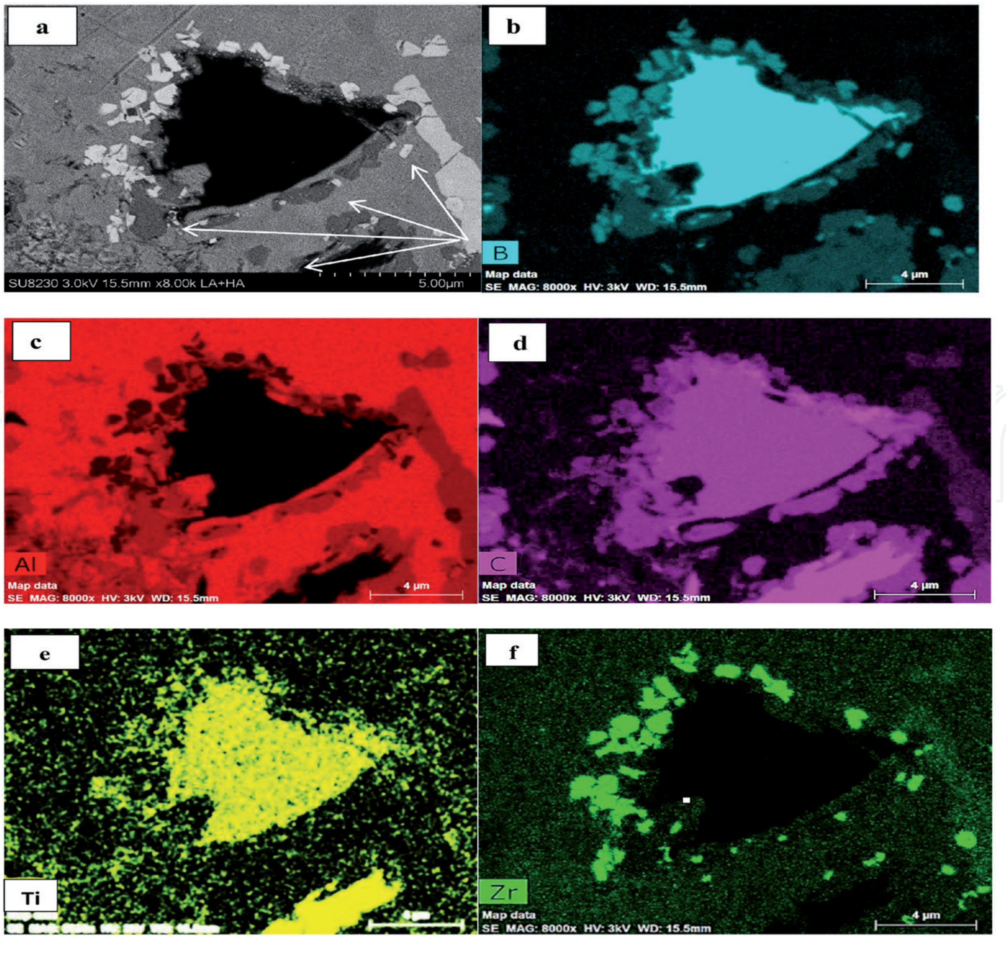

Figure 8.
Element distribution: (a) backscattered electron image-note formation of several particles around a B$_4$C particle, white arrows, (b) boron, (c) alumium, (d) carbon, (e) titanium, (f) zirconium.

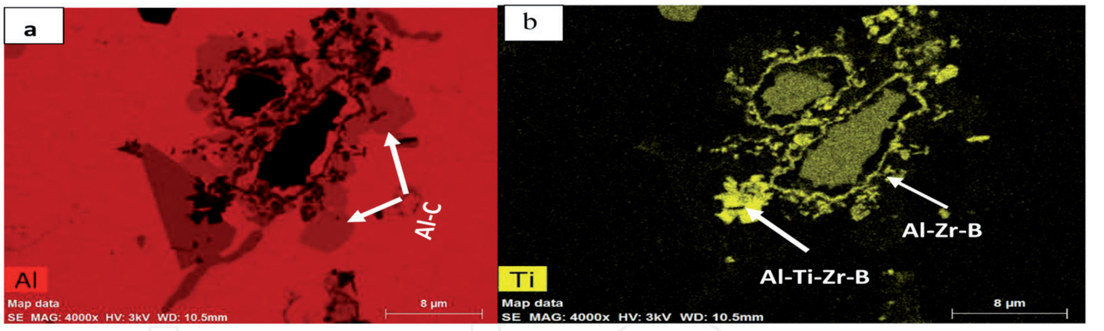

Figure 9.
B_4C-matrix interactions: (a) formation of Al-C, (b) formation of Zr rich phases-see ***Figure 7(c)*.**

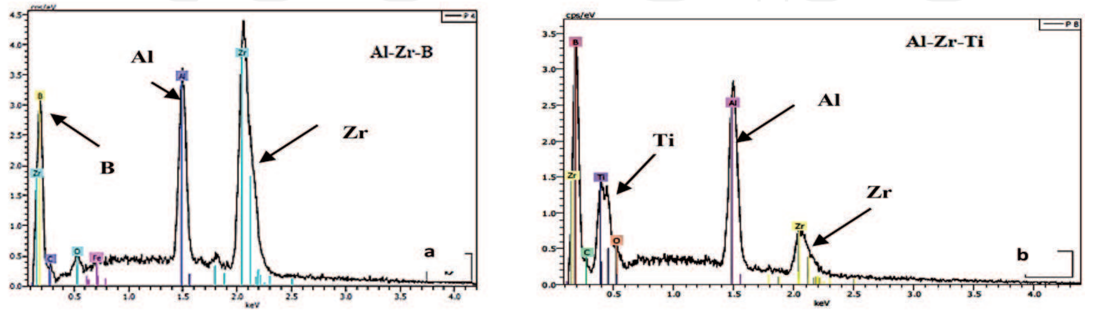

Figure 10.
EDS spectra obtained from ***Figure 9(b)*** *confirming the B4C-matrix interaction and the dependence of the composition of outcome on its position with respect to B4C particles.*

containing Ti and Zr. As can be seen in **Figure 7(a)**, the B_4C particles are surrounded by several layers of Zr–Ti rich phases (area marked I). Area marked II shows B_4C particles that have partially reacted with the matrix due to formation of the layer of AlBC existing in the matrix. In area III, fine B_4C particles are found be transformed completely into AlBC compounds. **Figure 7(b)** reveals a B_4C particle surrounded by a thin layer of Ti-rich phase followed by several layers of Zr–Ti rich phases. Some of these Zr–Ti rich phase particles are seen to grow into the aluminum matrix.

Figure 8 is produced from 5A composite remelted for multiple times at 730°C. **Figure 8(a)** shows the distribution of the B_4C particles. The B, Al and C distribution are presented in **Figures 8(b), 8(c), 8(d)**, respectively. Another point to be considered is that Ti covers the entire surface of the B_4C particle (similar to C and B) whereas Zr is limited to the layer decorating the B_4C particle. It is inferred from **Figure 9** that the layers surrounding the B_4C particles are a mixture of Al-Ti, and Al-C-Ti compounds. The EDS spectra obtained from **Figure 9(b)** are presented in **Figure 10**. Based on these EDSs, areas near the B_4C particles could be made of Al-B-Zr compound whereas those away are probably Al-Ti-Zr compound [55].

4. Mechanical properties

4.1 Impact testing

Total energies (Et) produced from the ten studied composites in the solutionized condition are shown in **Figure 11(a)**. Apparently the absorbed energy of the composite depends on what matrix is used and the volume fraction of the undissolved intermetallics. Following aging at 200°C for 10 h (**Figure 11(b)**), the precipitation of Zr-and Sc containing phases [55–58] led to significant decrease in the values of Et which may be attributed to precipitation of Mg_2Si phase particles

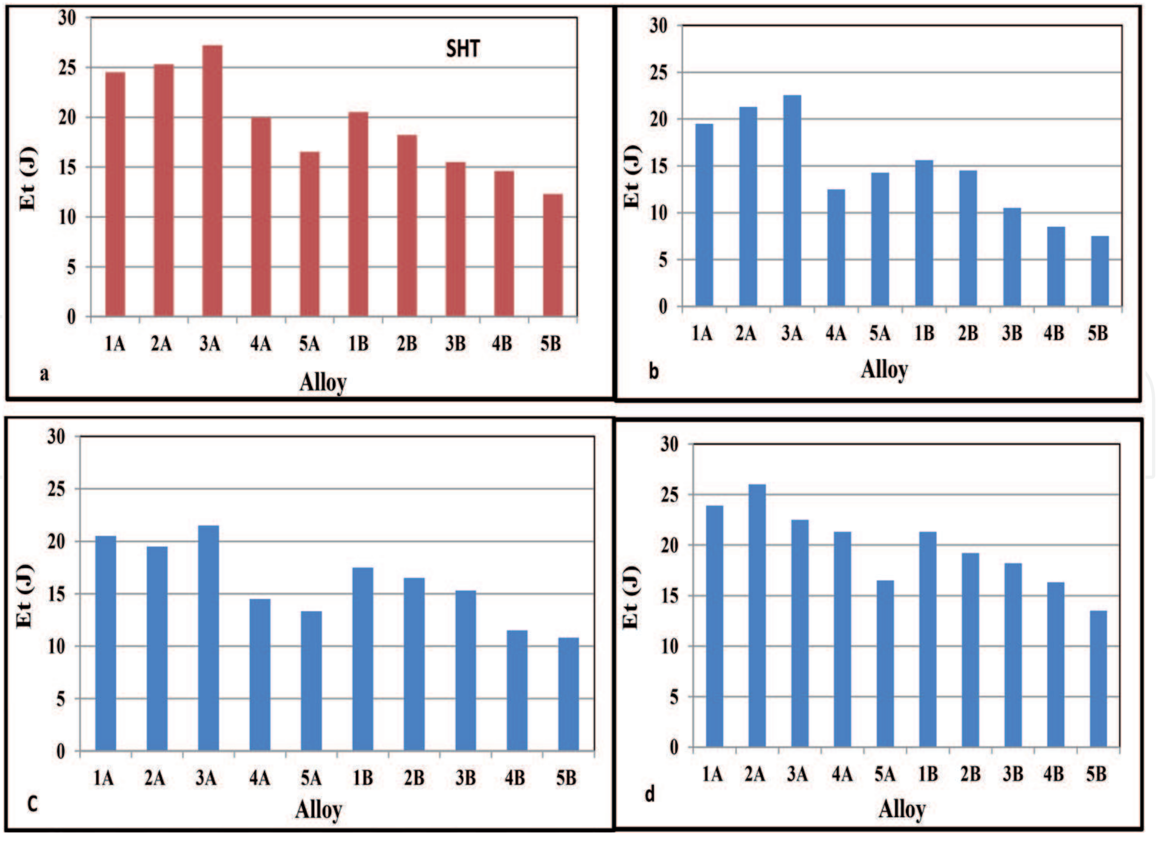

Figure 11.
Total absorbed energies of the present composites: (a) SHT, (b) aging at 200°C, (c) aging at 300°C, (d) aging at 400°C.

during aging in particular in B-series. It is inferred from **Figure 11(b)** that precipitation of Zr and/or Sc phases has an insignificant effect on the absorbed energy in series A-composites. According to Fuller et al. [59] aging 6063 alloy at 300°C would result in alloy softening due to coarsening of Mg_2Si phases particles. Simultaneous precipitation of Zr-rich phase may lead to balancing the composite toughness to some extent (**Figure 11(c)**). Aging at higher temperatures i.e. 400°C for 10 h resulted in coarsening of all types of precipitated phases causing important improvement in the composite toughness, regardless of the type of the matrix used, as exhibited in **Figure 11(d)**.

Fracture mechanism of Al-2%Cu composite was investigated by Miserez [60]. The study showed that the fracture may occur in two stages: (i) particle fracture leading to void nucleation in the matrix, and (ii) voids nucleated in the matrix in areas of high stress concentrations. The blue arrow in **Figure 12(a)** shows that the crack is propagating through the protecting layer surrounded by stacking faults (white arrows). On the left hand side of the micrograph several stacking faults appear in the form of steps (white arrows). Two distinctive types of cracks were observed in **Figure 12(b)**: cracks that took place at the interior of the B_4C particles and continued through the protecting layers i.e. intergranular, or those occurring at the B_4C/matrix interfaces (black arrow). No particle debonding was observed due to the existence of the protecting layers as displayed in **Figure 12(c)**. The microstructure beneath the fracture surface (vertical section-loading direction) shown in **Figure 12(d)** demonstrates the coherency between the B_4C particles and the surrounding matrix. Aging the composite at 400°C led to marked coarsening of the Al_3Zr phase particles as seen in **Figure 13(a)**, which explains the improvement in the composite toughness in **Figure 11(d)**. The EDS spectrum in **Figure 13(b)** corresponds to the circled area in **Figure 13(a)** revealing strong reflections from Al and Zr elements.

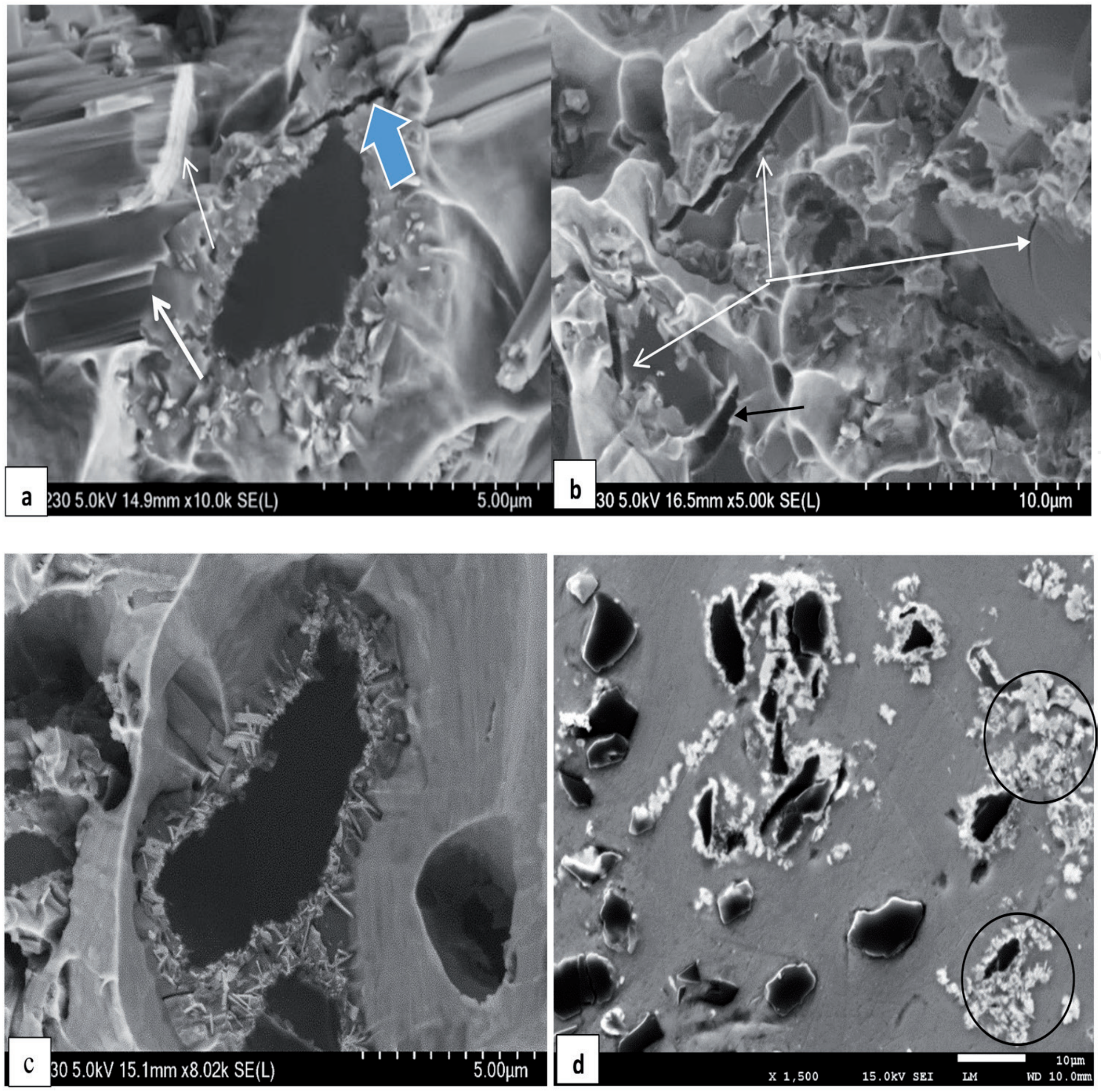

Figure 12.
Fracture characteristics of the present composites: (a) stacking faults-SHT, (b) cracks- aging at 200°C/10 h, (c) B_4C/matrix coherency, (d) vertical section beneath (c) confirming particle/matrix bonding-note the severe reaction around some of the B_4C particles - circled areas.

4.2 Tensile testing

4.2.1 Room temperature testing

The stress–strain curves of two aluminum matrix composites in the SHT condition and after aging at 200°C/h are shown in **Figure 14**. The main observation to be made is the slow working hardening rate illustrated by low work hardening and the slow increase in the composite UTS (**Figure 14(a)**). As a consequence of aging at 200°C/10 h, the UTS increased by approximately 80 MPa which may be attributed to the precipitation of Al_3Zr phase particles [61]. Considering the solutionizing treatment of 5B composite the maximum attainable strength is about 280 MPa- **Figure 14(b)**. Using a heat treatable matrix i.e. 6063 alloy, the composite revealed significant improvement in both the UTS levels as well as work hardening rate as displayed in **Figure 14(c)** which may be caused by the precipitation of Mg_2Si phase particles during the storing period prior to testing (~10 minutes at room temperature). As expected, aging at 200°C/10 h resulted in increasing the composite strength from 280 MPa to 500 MPa, **Figure 14(d)**, which may be interpreted in terms of simultaneous precipitation of both Mg_2Si and Al_3Zr phase particles.

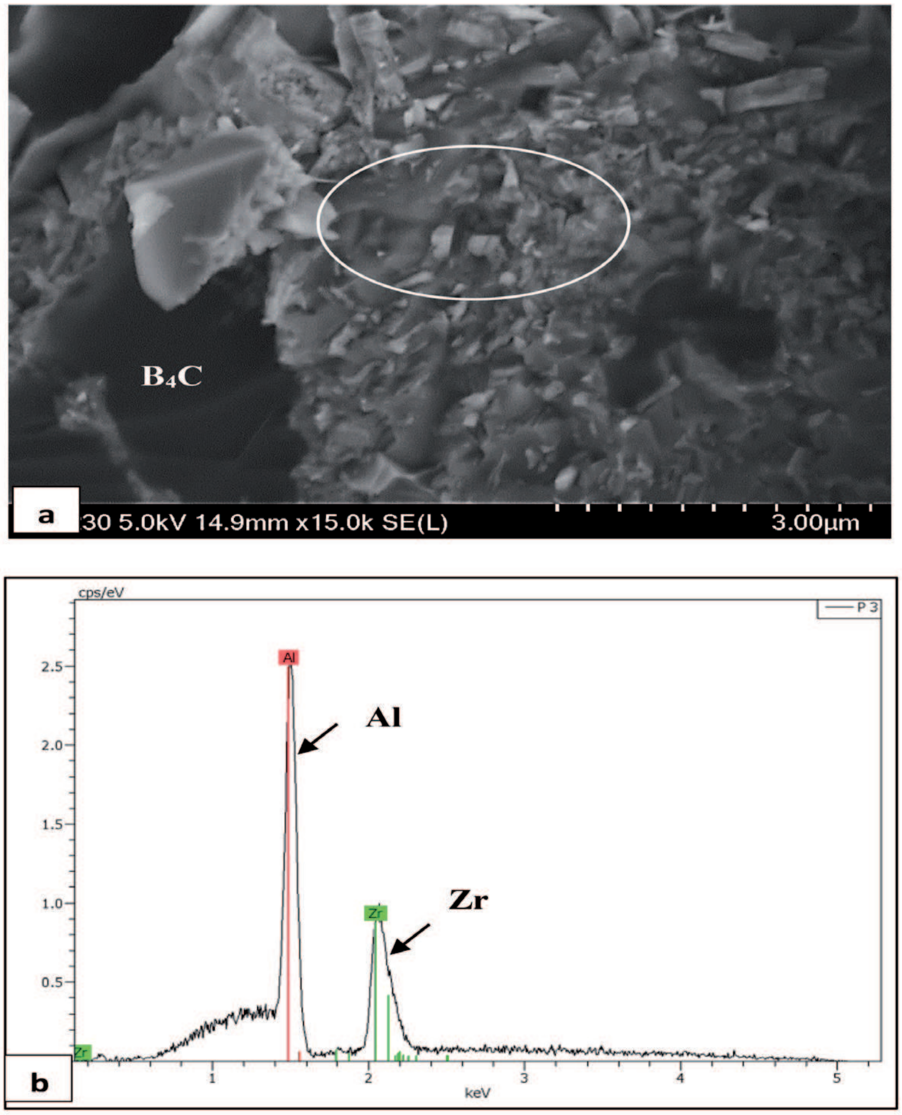

Figure 13.
(a) Fracture surface of composite 5B aged at 400°C/10 h, (b) EDS spectrum corresponding to white circle in (a).

Following the solution heat treatment of composite 5A, the fracture surface is characterized by the formation of deep dimple network as demonstrated in **Figure 15(a)**. Some of these dimples revealed the presence of deformation bands (arrowed) due to composite ductility. The marking seen on the surface of the B_4C particles in **Figure 15(b)** may be caused by gradual fracture of the particles, maintaining at the same time their coherency with the aluminum matrix. Precipitation of Al_3Zr phase particles during aging at 200°C/10 h is clearly seen in **Figure 15(c)**. Due to reduction in the composite ductility, some of the B_4C particles were cracked as shown by the white arrows in the same figure. In the case of 6063 alloy matrix, with the significant increase in the composite UTS level following aging at 200 C/10 h (500 MPa), cracks are seen to initiate and propagate through the Zr-Ti protecting layer as demonstrated in **Figure 15(d)** – see blue arrow. No B_4C particle debonding is observed to take place under axial loading.

4.2.2 High temperature testing

The 5A and 5B composites (**Table 1**) were tested in the temperature range of 25–500°C and their corresponding stress–strain curves are displayed in **Figure 16**. Composite 5B showed a slightly higher strength compared to composite 5A. It should

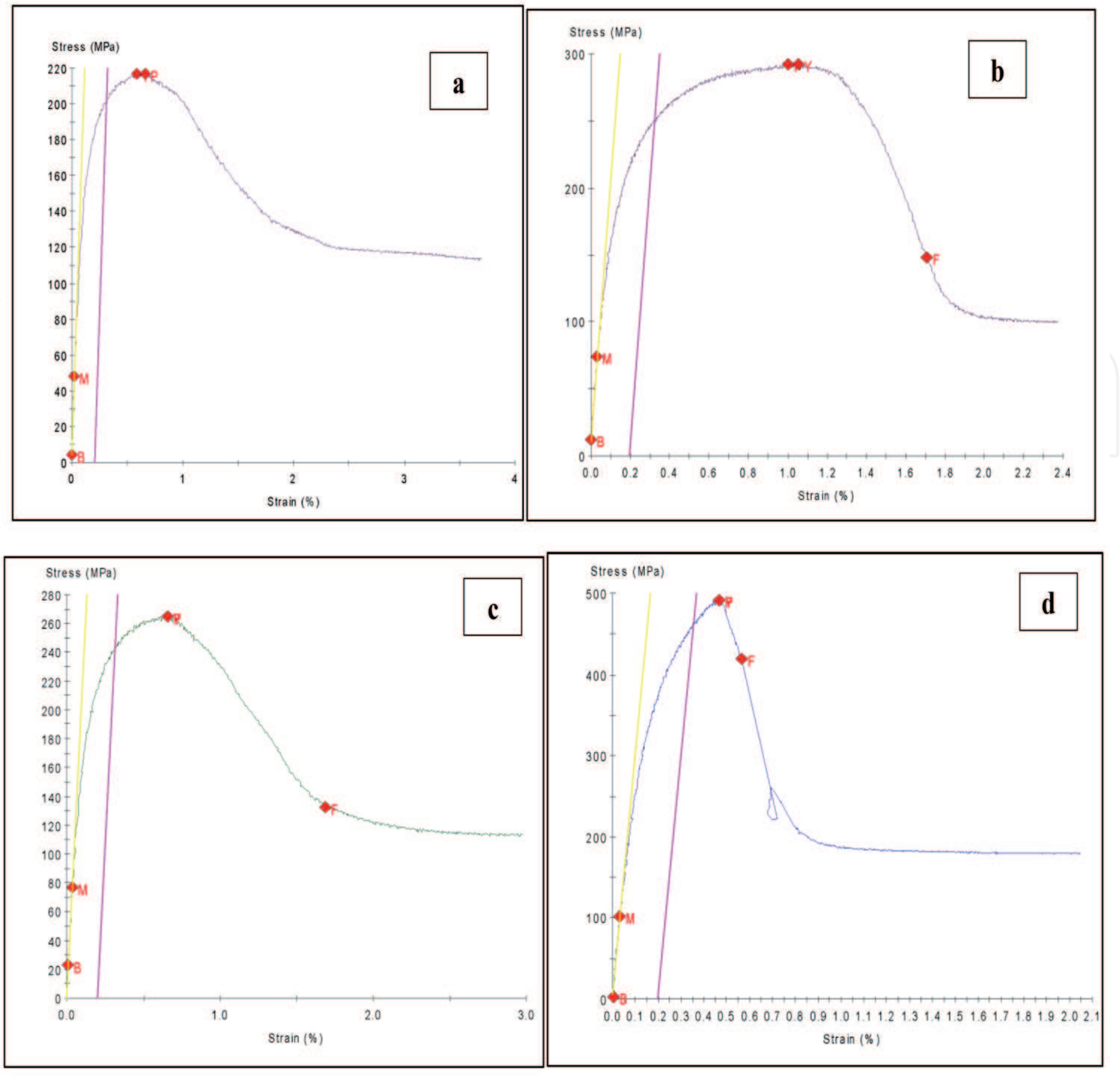

Figure 14.
Stress–strain diagrams corresponding to: (a) Al/B_4C 5A composite - SHT, (b) Al/B_4C composite aged at 200°C/ 10 h, (c) 5B 6063/B_4C composite - SHT, (d) 6063/B_4C composite aged at 200°C/ 10 h.

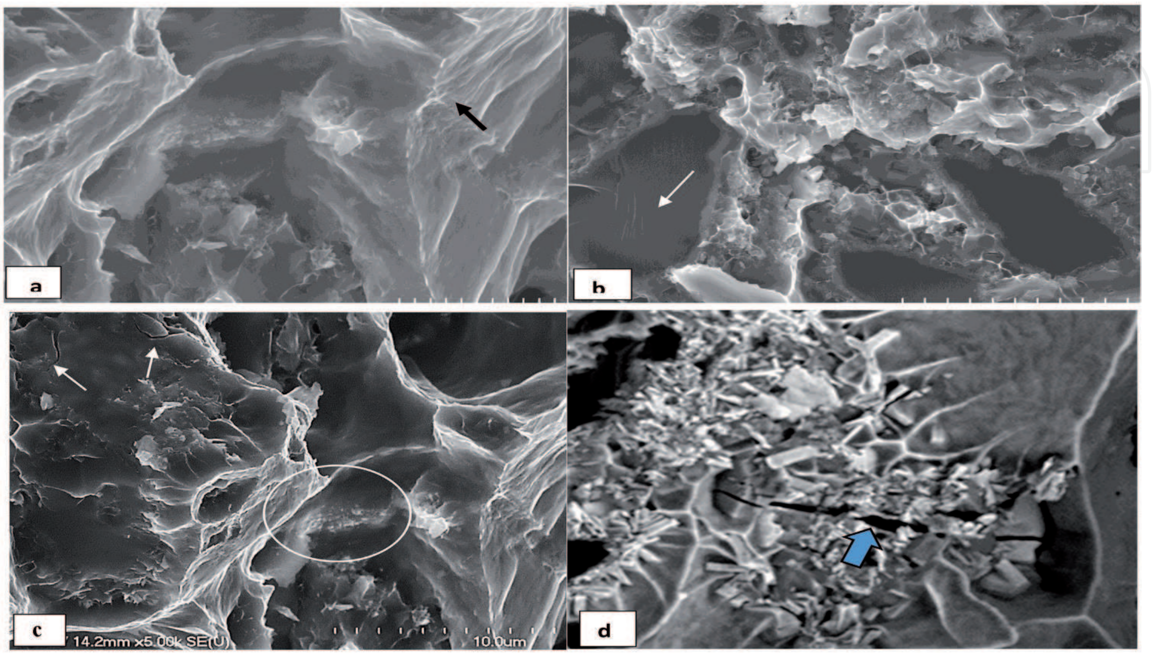

Figure 15.
Fracture surface of tensile tested samples of 5A composite: (a,b) SHT, (c,d) aging at 200 C/10h.

be mentioned here that samples of composite 5B were tested in the T4 condition which involves natural aging. Increasing the testing temperature up to 450°C resulted in significant increase in the composite pct. Elongation to failure. Aging at further higher temperature would lead to precipitation of Al_3Zr which would result in reducing the composite ductility, as shown in **Figure 16(c)** [6, 62–65].

For aging at temperatures higher than 0.5 of the melting temperature (Tm), there is a similarity between creep and hot deformation. Under this condition, the relation between the measured parameters can be expressed using power law relationships as described by Eq. 1 [66–70]:

$$\dot{\varepsilon}\exp\left(\frac{Q_a}{RT}\right) = A\sigma^n = Z \tag{1}$$

where $\varepsilon^{\cdot}$ = strain rate, σ = flow stress, n = stress exponent, Q_a = activation energy, R = gas constant, T = absolute temperature, A is a constant and Z = Zener-Hollomon parameter. At a constant $\varepsilon^{\cdot}$, σ^n can expressed as:

$$\sigma^n = B\exp\left(\frac{Q_a}{RT}\right) \tag{2}$$

where B = constant. Differentiation of Eq. 2 coupled with (1/T), gives Q_a as:

$$\frac{\partial \ln\sigma}{\partial\left(1/T\right)} = \frac{Q_a}{nR} \tag{3}$$

Applying these equations, the plot of lnσ *vs* 1/T, will give a straight line with a slope of (Q_a/nR) as shown in **Figure 17** [66–68].

The fracture surface of composite 5A tested at 25°C was characterized by the presence of deformation bands covering the internal surface of the dimples as shown previously. **Figure 18(a)** exhibits the fracture surface of 5A composite tested at 250°C revealing multiple contour-type markings (white arrow) due to the high ductility ~15%. Testing at 350°C resulted in major increase in the deformation bands in the form of steps (blue arrows) as shown in **Figure 18(b)**. The thin white arrows point to cracked B4C particles. The black arrow in **Figure 18(c)** - 5A composite pulled to fracture at 450°C- indicates the presence of a long crack within the protective layer. In addition, the 5A composite exhibited elongated dimples as depicted in **Figure 18(c)**. **Figure 18(d)** is an enlarged portion of the crack in **Figure 18(c)**.From the associated EDS spectrum in **Figure 18(e)**, the possibility of precipitation of a large amount of Zr-rich particles, which would explain the reduction in the composite ductility when tested at this temperature. Fractographic observations made by Zhang et al. [69] on 6092/(B_4C)p indicated the possibility of several interfacial bonding characteristics such as good bonding (extruded composites) and weak bonding (hot isostatic pressing). The fracture surfaces of composites would also show a mixture of ductile and brittle types of fracture [70].

The fracture surface of 5B composite pulled to fracture at 250°C revealed that in addition to the deep dimples, some stacking faults could also be seen in the fracture surface (**Figure 19(a)**-white arrows). As in the case of 5A composite, at 350°C, the fracture surface exhibited a well-defined dimple structure as a result of the increase in the composite % elongation to fracture, **Figure 19(b)**-black arrows point to the thickness of the protection layer. Due to the strong particle/matrix interface adhesion, some of the B_4C particles have been cracked at their interior. In this case, the crack was initiated at the particle/matrix interface and propagated through the particle. When the sample was tested at 450°C, the fracture surface revealed the formation of very large and deep dimple network as shown in **Figure 19(c)**.

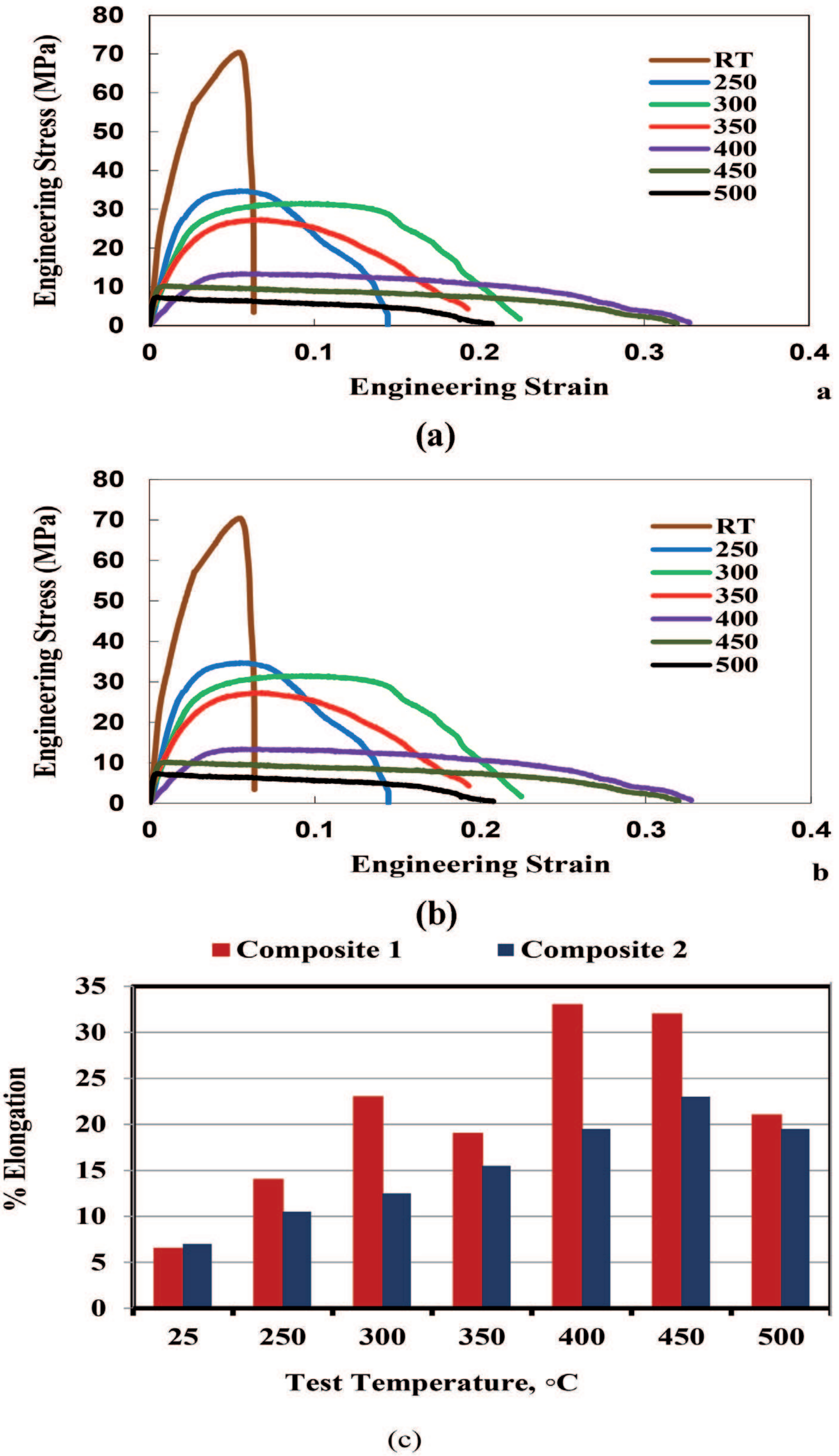

Figure 16.
(a) Stress–strain curves obtained from 5A composite, (b) stress–strain curves obtained from 5B composite, (c) % elongation as a function of testing temperatire (composite 1 is 5A, composite 2 is 5B).

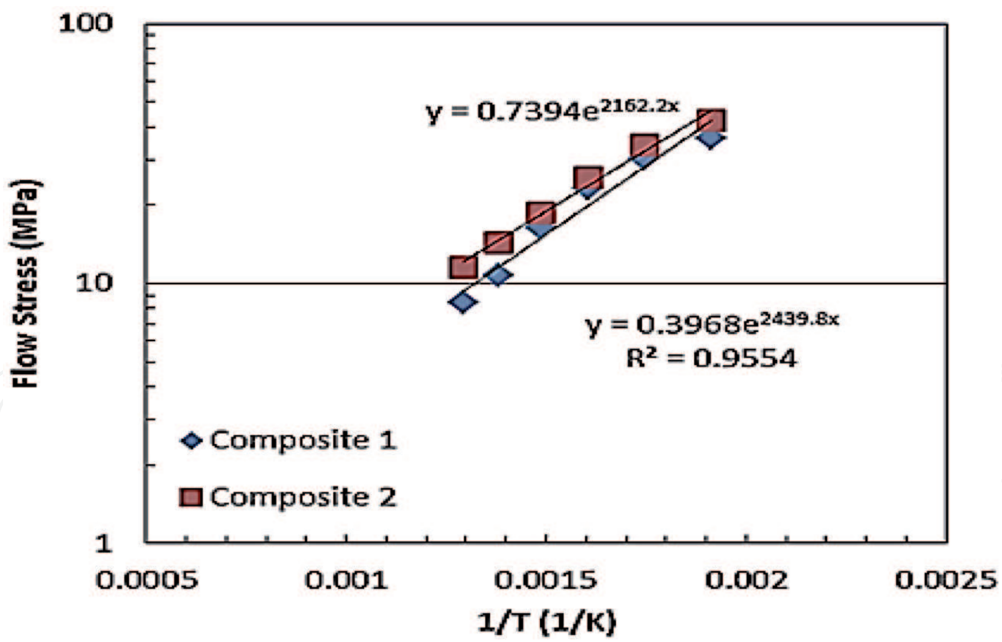

Figure 17.
Relationship of flow stress vs 1/T (T = in kelvin degree).

4.2.3 Effect of strain rate

The main characterized parameters of hot deformation or creep behavior of commercial Al alloys and Al-based composites are by high values of n_a (> 5) as well as the activation energy Q_a. These values are higher than those for solute diffusion [71–75]. This behavior can be explained in terms of interaction of dislocations with the dispersed strengthening particles resulting in a threshold stress σ_o. In this case, the deformation process is related to an effective stress, $\sigma_e = (\sigma - \sigma_o)$ not the applied stress σ. Therefore, equations 1-2 can be rewritten to take into consideration σ_o as follows

$$\dot{\varepsilon}\exp\left(Q_t / RT\right) = Z = A'\frac{Gb}{kT}\left(\frac{\sigma - \sigma_0}{G}\right)^{n_t} \tag{4}$$

where: A = constant, k = Boltzmann's constant, b = magnitude of Burgers vector, G = shear modulus and Q_t = true activation energy.

The true stress–strain curves obtained from testing the 5A composite tested at 300°C (a), 400°C (b) and 500°C (c), are respectively depicted in **Figure 20**. These curves can be divided into three stages; strain hardening where the stress increases with strain until reaches a steady state. Stage 2 represents maximum stress, followed stage 3 where necking takes place leading to failure. Generally speaking, with increasing the strain rate would result in an increase in the flow stress. The effect of testing temperature on the behavior of the stress- strain curves at a constant strain rate of 10^{-3} s^{-1} is displayed in **Figure 20(d)**. Increasing the testing temperature led to an increase in the composite ductility at 500°C and higher strain rates higher than 10^{-2} s^{-1}. The ductility was decreased in temperature range of 350° C–450°C.

The relationship between the strain rate, $\dot{\varepsilon}$ and stress σ, at a constant temperature, is governed by plotting $\dot{\varepsilon}$ *vs.* σ applying a log log scale (**Figure 21**) for different testing temperatures. The results reported in **Figure 20** may suggest that the data points at each testing temperature fall on a straight line with a constant na that increases from 5.8 at 500°C to ~7 at 350–450°C, thereafter to 10.4 at 300°C. The high values of n_a are close to those obtained for commercial aluminum alloys [76–80] and metal matrix composites. As mentioned before, dislocations -second phase

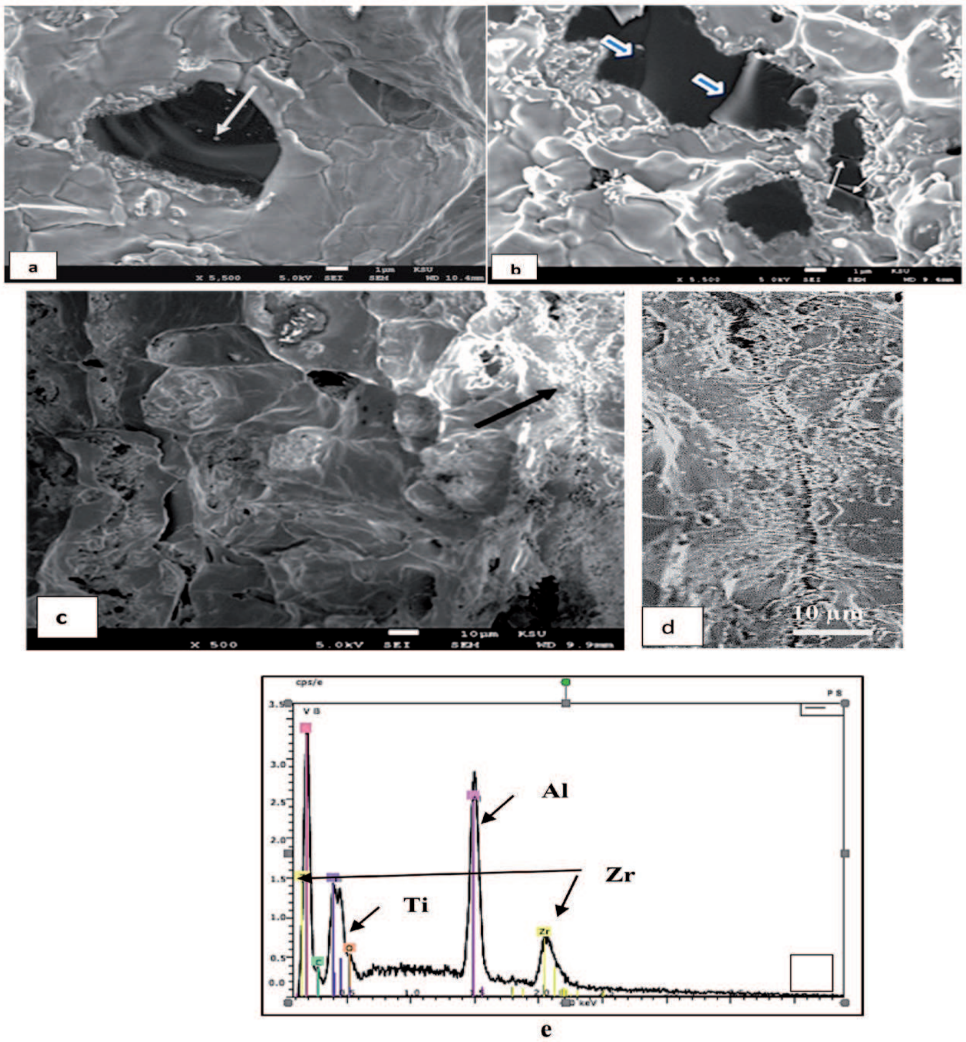

Figure 18.
Fracture surface of tensile tested samples of 5A composite: (a) 250°C, (b) 350°C, (c) 450 C, (d) an enlarged portion of (c) showing the crack, (e) EDS corresponding to (c) revealing reflections due to Al, Zr, Ti elements.

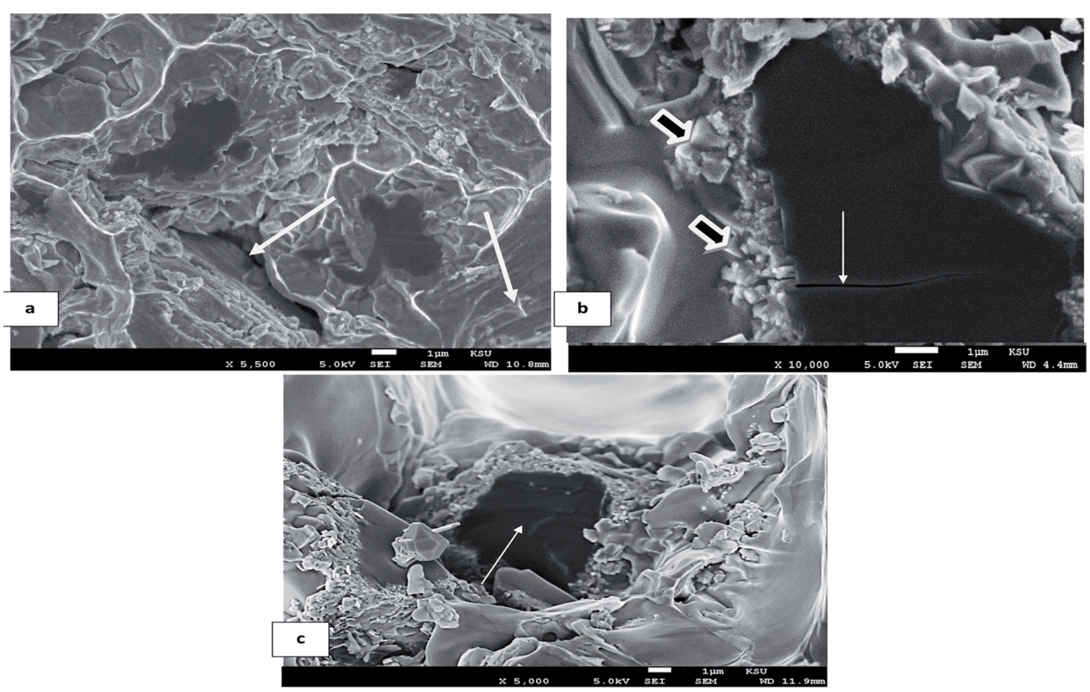

Figure 19.
Fracture behavior of 5B composite tested at: (a) 250°C, (b) 350°C, (c) 450°C.

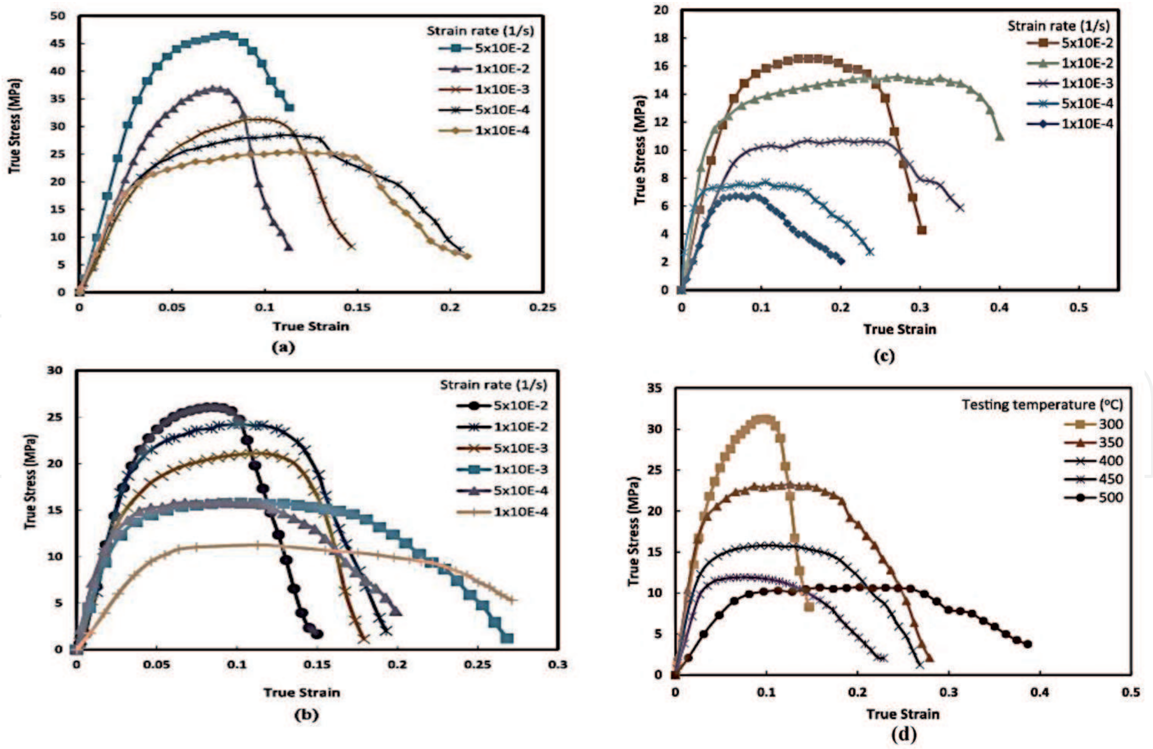

Figure 20.
True stress–strain curves at different strain rates at (a) 300°C, (b) 400°C, (c) 500°C, (d) strain rate 10^{-3} s^{-1}.

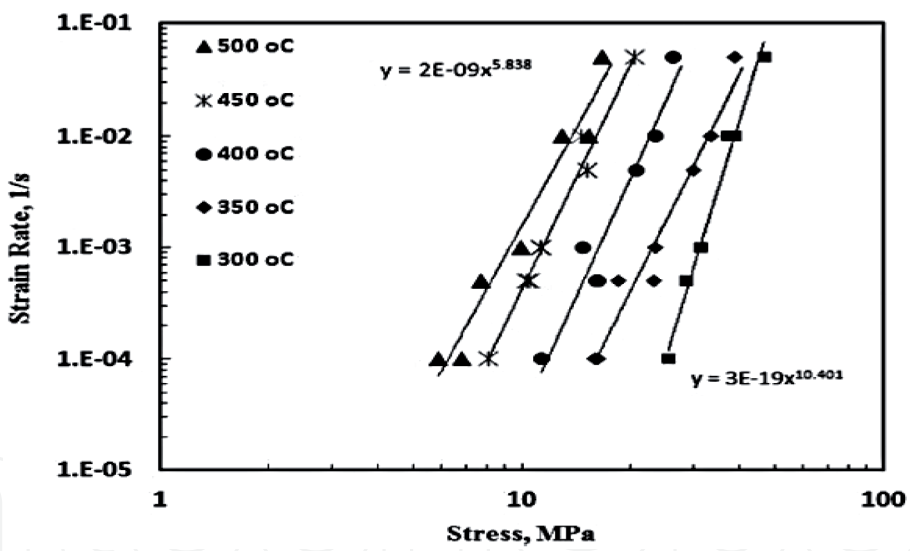

Figure 21.
Strain rate and stress relationship in the temperature range 300–500°C.

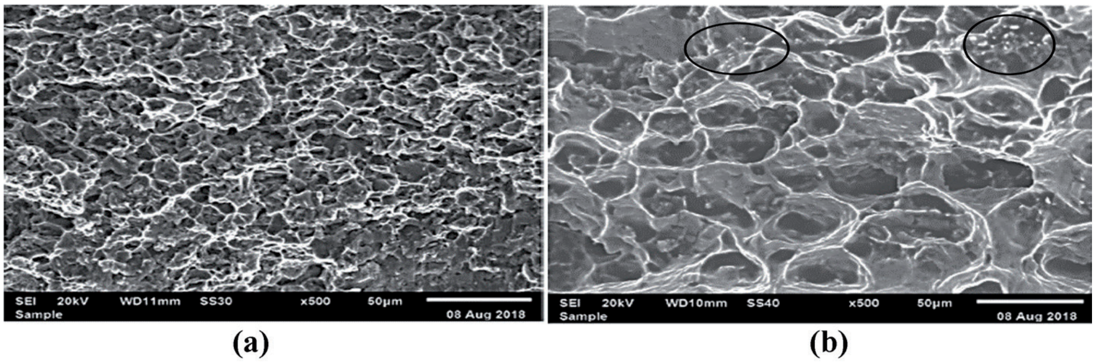

Figure 22.
Fracture surface of samples tested at 300°C: (a) 10^{-2} s^{-1}, (b) 10^{-4} s^{-1}.

particles interaction would lead to high values of n_a and Q_a threshold stress in the composite materials.

Figure 22 (a) shows the fracture surface of the samples tested at 300°C (strain rate of 10^{-2} s^{-1}), consisting of a mixture of small dimples and intragranular fracture. **Figure 22 (b)** is the fracture surface at strain rate of 10^{-4} s^{-1} at 300°C, exhibiting larger dimples with precipitation of Al_3Zr in particles at their interiors (circled areas) [81].

5. Summary

The results obtained from the present investigations revealed that the powder injection technique used in our study proved to be effective in producing composites with a uniform distribution of B_4C particles throughout the matrix (commercial aluminum or 6063 alloy). The combined addition of Zr and Ti improved the possibility of increasing the number of B_4C particles in the matrix by improving the particulate wettability. The precipitating $Al_3(Zr_{1-x}Ti_x)$ particles decorating the B_4C particles were found to grow into the surrounding matrix. Precipitation of Mg_2Si in 6063/B_4C was more effective in controlling the composite toughness than Al_3Zr in the under-aging conditions. Overaging occurred at 400°C for prolonged aging times (i.e. 10 h), resulting in a significant improvement in the composite toughness regardless the type of the matrix. Cracks were always initiated at the particle/matrix interfaces and propagated either through the B_4C particles or along the protecting $Al_3(Zr_{1-x}Ti_x)$ layer. No particle debonding was observed regardless the type of matrix or the testing method. Formation of the Zr/Ti rich layers surrounding the B_4C particles strengthen their adhesion to the surrounding matrix. Increasing the testing temperature leads to rapid decrease in the composite strength in an exponential pattern which appeared in the gradual fracturing of the reinforcement B_4C particles. The plots of flow stress as a function of testing temperature are linear with a fitting factor of 0.955. The value of n_t ~ 5 and Q_t of 130 kJ mol^{-1} along with subgrain formation may conclude that dislocation climb is the main controlling process. Similar observation was made in pure Al with dispersed particles. The pct elongation to failure reached a maximum value at intermediate value of Z, which can determine the optimum conditions for the composite formability.

Author details

Mohamed F. Ibrahim[1]*, Hany R. Ammar[2], Agnes M. Samuel[1],
Mahmoud S. Soliman[3], Victor Songmene[4] and Fawzy H. Samuel[1]

1 Université du Québec à Chicoutimi, Chicoutimi, Québec, G7H 2B1, Canada

2 Department of Mechanical Engineering, Qassim University, Saudi Arabia

3 Department of Mechanical Engineering, King Saud University, Riyadh, Saudi Arabia

4 Department of Mechanical Eng., École de Technologie Supérieure, Québec, Canada

*Address all correspondence to: fhsamuel@uqac.ca

References

[1] K. Kalaiselvan, N. Murugan, S. Parameswaran, Production and characterization of AA6061–B4C stir cast composite, Materials and Design, 32 (2011), pp. 4004-4009.

[2] S. Roy, S. Sharma, S. Sharma, Review on Fabrication of Aluminum 7075+ B4C Composites and its Testing, Int. J. of Advanced Research in Science and Eng., 6(2017), pp. 647-652.

[3] K.E. Öksüz and K.O. Oskay, The Effects of Aging on the Hardness and Wear Behaviour of 2124 Al Alloy/B4C Composites, Proceedings of the 4th International Congress APMAS2014, April 24-27, 2014, Fethiye, Turkey, 127 (2015), pp. 1367-1369.

[4] A. Singla, S. Shandilya, P. Gera, A. Gupta, Process Parameter Optimization using DOE Methodology on Al- MMC to Maximize Mechanical Properties, International Journal of Emerging Science and Engineering (IJESE), ISSN: 2319-6378, Volume-5 Issue-2, January 2018, pp. 4-7.

[5] S. Mohan, E. Kennedy, MACHINABILITY STUDIES OF ALSIB4C DEVELOPED MMC DEVELOPED USING STIR CASTING, Journal of Engineering & Technology, 4(2014), pp. 25-28.

[6] R.U. Vaidya, S.G. Song, A.K. Zurek, Dynamic mechanical response and thermal expansion of ceramic particle reinforced aluminum 6061 matrix composites. Philos Mag A, 70 (1994): pp. 819-836.

[7] Y. Kumar, G. Anil Kumar, J. Satheesh, T. Madhusudhan, A Review On Properties Of Al-B4C Composite Of Different Routes, International Research Journal of Engineering and Technology, 3 (2016), pp. 860-865.

[8] İ. Topcu, Investigation of Wear Behavior of Particle Reinforced AL/B4C Composites under Different Sintering Conditions, TEHNIČKI GLASNIK 14, (2020), pp. 7-14.

[9] B. Manjunatha, H. B. Niranjan, K.G.Satyanarayana, Effect of amount of boron carbide on wear loss of Al-6061 matrix composite by Taguchi technique and Response surface analysis. Materials Science and Engineering, 376(2018), https://doi.org/10.1088/1757-899X/376/1/012071.

[10] K.M. Shorowordi , A.S.M.A. Haseeb J.P. Celis, Tribo-surface characteristics of Al–B4C and Al–SiC composites worn under different contact pressures, Wear, 261 (2006), pp. 634-641.

[11] K.M. Shorowordi, T. Laoui, A.S.M.A. Haseeb, J.P. Celis, L. royen, Microstructure and interface characteristics of B4C, SiC and Al2O3 reinforced Al matrix composites: a comparative study, J.Mater. Process. Technol. 142 (2003), pp. 738-743.

[12] K.M. Shorowordi, A.S.M.A. Haseeb, J.P. Celis, Velocity effects on the wear, friction and tribochemistry of aluminium MMC sliding against phenolic brake pad, Wear 256 (2004)pp. 1176-1181.

[13] G. Straffellini, M. Pellizzari, A. Molinari, Influence of load and temperature on the dry sliding behaviour of Al-based metal-matrix-composites against friction material, Wear 256 (2004), pp.754-763.

[14] M. Sing, D.P. Mondal, O.P. Modi, A.K. Jha, Two-body abrasive wear behaviour of aluminum alloy–sillimanite particle reinforced composite, Wear, 253 (2002),pp. 357-368.

[15] R.M. Mohanty, K. Balasubramaniam, S.K. Seshadri,

"Boron-Carbide Reinforced Aluminium 1100 matrix composites: Fabrications and properties", Materials Science and Engineering A, 498, (2008), pp. 42-52.

[16] A. Canakci "Microstructure and abrasive wear behavior of B4C particle reinforced 2014 Al matrix composites", J. Mater. Sci., 46 (2011),pp. 2805-2813.

[17] I. Kerti and F. Toptan , Microstructural variations in cast B4C-reinforced aluminum matrix composites (AMCs), Mater Lett, 62, (2008). P.1215.

[18] V. Auradia, G.L. Rajesh, S. A. Kori, Processing of B4C Particulate Reinforced 6061Aluminum Matrix Composites by melt stirring involving two-step addition, Procedia Materials Science, 6 (2014), pp.1068-1076.

[19] A.R. Kennedy, B. Brampto, The reactive wetting and incorporation of B4C particles into molten aluminum, Scripta Mater, 44, (2014), pp.1077-1082.

[20] H.O. Topcua, N. Gulsoy A.N. Kadiogluc, Gulluoglua, "Processing and mechanical properties of B4Creinforced Al matrix composites", J. Alloys Compd. 482 (2009), 516.

[21] I. Topcua, H.O. Gulsoy, N. Kadioglu, A.N. Gulluoglu, Processing and mechanical properties of B4C reinforced Al matrix composites, Journal of Alloys and Compounds,482(2009), pp. 516-521.

[22] K. Kalaiselvan, N.Murugan, S. Parameswaran, Production and characterization of AA6061–B4C stir cast composite, Materials & Design, 32(2011), pp. 4004-4009.

[23] M. Uthayakumar, S. Aravindan, K. Rajkumar, Wear performance of Al–SiC–B4C hybrid composites under dry sliding conditions, Materials and Design 47 (2013), pp. 456-464.

[24] Y. Mazaheri, M. Meratian, R. Emadi, A.R. Najarian, "Comparison of microstructural and mechanical properties of Al–TiC, Al–B4C and Al–TiC–B4C composites prepared by casting techniques" Materials Science & Engineering A, 560 (2013),pp. 278-287.

[25] F. Toptan, A. Kilicarslan, I. Kerti, The Effect of Ti Addition on the Properties of Al-B4C Interface: A Microstructural Study, Materials Science Forum, 636-637 (2010), pp. 192-197.

[26] R. Ipek, Adhesive wear behaviour of B4C and SiC reinforced 4147 Al matrix composites (Al/B4C–Al/SiC), J. Mater. Procng. Technol, 162-163 (2005), pp. 71-75.

[27] F. Bedir, Characteristic properties of Al–Cu–SiCp and Al–Cu–B4Cp composites produced by hot pressing method under nitrogen atmosphere, Mater. & Design 28 (2007) 1238-1244.

[28] M. Aizenshtein, N.Froumin, E. Shapiro-Tsoref, M.P. Dariel, N. Frage, Wetting and interface phenomena in the B4C/(Cu–B–Si) system, Scripta Mater. 53 (2005), pp. 1231-1235.

[29] J. Jung and S. Kang, Advances in Manufacturing Boron Carbide–Aluminum Composites, J. Am. Ceram. Soc., 87(2004), pp.47-54.

[30] P. Shen, B. Zou, S. Jin, Q. Jiang, Reaction mechanism in self-propagating high temperature synthesis of TiC-TiB2/Al composites from an Al-Ti-B4C system, Mater. Sci. & Eng. A 454-455 (2007), pp. 300-309.

[31] P.Kumar and R. Parkash, Experimental investigation and optimization of EDM process parameters for machining of aluminum boron carbide (Al–B4C) composite, Machining Science and Technology, 20 (2016), 330-348.

[32] Wang HY, Jiang QC, Wang Y, Ma BX, Zhao F. Fabrication of TiB2 particulate reinforced magnesium matrix composites by powder metallurgy. Mater Lett 58(2004), pp.3509-3513.

[33] H. Yang, T. D. Topping, K. Wehage, L. Jiang, E. J. Lavernia, J. M. Schoenung, Tensile behavior and strengthening mechanisms in a submicron B4C-reinforced Al trimodal composite, Materials Science and Engineering: A, 616 (2014), pp. 35-43.

[34] A. Yazdani and E. Salahinejad, Evolution of reinforcement distribution in Al–B4C composites during accumulative roll bonding, Materials and Design 32 (2011), pp. 3137-3142.

[35] H. Junaedi, M.F.A. Ibrahim, H.R. Ammar, A.M. Samuel, M.S. Soliman, A.A. Almajid, and F.H. Samuel, Effect of testing temperature on the strength and fracture behavior of Al-B4C composites. Journal of Composite Materials, 50(2016): pp. 2871-2880.

[36] M.F. Ibrahim, H.R. Ammar, A.M. Samuel, M.S. Soliman and F.H. Samuel, On the impact toughness of Al-15 vol.% B4C metal matrix composites. Composites Part B: Engineering, 2015. 79 (2015): pp. 83-94.

[37] M.F. Ibrahim, A.M. Samuel, F.H. Samuel, H.R. Ammar and M.S. Soliman, On the Impact Toughness of Al-B4C MMC: The Role of Minor Additives and Heat Treatment, in 119th Metalcasting Congress, AFS 2015, Columbus, OH, April 21-23, 2015. 2015, American Foudry Society: Columbus, Ohio.

[38] M.F. Ibrahim, H.R. Ammar, A.M. Samuel, M.S. Soliman, A.A. Almajid, and F.H. Samuel, Mechanical properties and fracture of Al-15 vol.-%B4C based metal matrix composites. International Journal of Cast Metals Research, 27(2014): pp. 7-14.

[39] M.F. Ibrahim, H.R. Ammar, A.M. Samuel, M.S. Soliman and F.H. Samuel, Neue technologie zur produktion von Al-B4C Metalmatrix-verbundwerkstoffen. Giesserei Praxis, 6(2014): pp. 263-271.

[40] M.F. Ibrahim, A.M. Samuel, H.R. Ammar, M.S. Soliman and F.H. Samuel, A new technology for the production of Al-B4C metal matrix composites. Giesserei-Praxis, 65(2014): pp. 263-271.

[41] M.F. Ibrahim, H.R. Ammar, S.A. Alkahtani and F.H. Samuel, Metallographic investigation of tensile- and impact-tested aluminum composites. Journal of Composite Materials, 2016. 50(20): p. 2793-2805.

[42] M.F. Ibrahim, H.R. Ammar, A.M. Samuel, M.S. Soliman and F.H. Samuel, Metallurgical parameters controlling matrix/B4C particulate interaction in aluminium-boron carbide metal matrix composites. International Journal of Cast Metals Research, 26(2013): pp. 364-373.

[43] M.F. Ibrahim, A.M. Samuel, H.R. Ammar, M.S. Soliman and F.H. Samuel, A New Technology for the Production of Al-B4C Metal Matrix Composites, in Transactions of the American Foundry Society volume 121; 117th Metalcasting Congress ; April 6-9, 2013, [St. Louis, Missouri ; in conjunction with CastExpo'13]. 2013, American Foundry Society: [St. Louis, Missouri; in conjunction with CastExpo'13]. p. 99-110.

[44] M. S. Soliman, M. M. El Rayes, A. T. Abbas, D. Yu. Pimenov, I. N. Erdakov, H. Junaedi, Effect of tensile strain rate on high-temperature deformation and fracture of rolled Al-15 vol% B4C composite, Materials Science & Engineering A, 749(2019), pp.129-136.

[45] A. J. Pyzik, R. A. Newman, A. Wetzel and E. Dubensky: 'Composition control in aluminum boron carbide

composites,' in 'Mechanical properties and performance of engineering ceramics II: ceramic engineering and science proceedings', (ed. R. Tandon et al.), Vol. 27; 2007, Westerville, OH, American Ceramic Society.

[46] X. G. Chen: 'Application of Al–B4C metal matrix composites in the nuclear industry for neutron absorber materials', Proc. On 'Solidification processing of metal matrix composites', San Antonio, TX, USA, March 13-16, 2006 TMS, pp.343-350.

[47] M. C. Flemings: 'Fluidity of metals – techniques for producing ultra-thin section castings', Br. Foundryman, 57(1964), pp.312-325.

[48] M. Rosso, Ceramic and metal matrix composites: Routes and properties, Journal of Materials Processing Technology, 175(2006), pp.364-375.

[49] H. Tahiri: 'Affinement des grains des alliages Al-(0-17%)Si', PhD thesis, Université du Québec à Chicoutimi, Chicoutimi, Que., Canada, 2007.

[50] H. Tahiri, S.S. Mohamed, H.W. Doty, S. Valtierra and F.H. Samuel, Effect of Sr–Grain Refining–Si Interactions on the Microstructural Characteristics of Al–Si Hypoeutectic Alloys. International Journal of Metalcasting, 12(2018): pp. 343-361.

[51] H. Tahiri, A.M. Samuel, H.W. Doty, S. Valtierra and F.H. Samuel, Effect of Sr–Grain Refiner–Si Interactions on the Microstructure Characteristics of Al–Si Hypereutectic Alloys. International Journal of Metalcasting, 12(2018): p. 307-320.

[52] H. Tahiri, S.S. Mohamed, H.W. Doty, S. Valtierra and F.H. Samuel, Effects of Grain Refining on Columnar-to-Equiaxed Transition in Aluminum Alloys, in Aluminum Alloys - Recent Trends in Processing, Characterization, Mechanical Behavior and Applications, S. Sivasankaran, Editor. 2017, InTech.

[53] H. Tahiri, F.H. Samuel and A.M. Samuel, Grain refinement in modified A356 Alloy, in 18th Canadian Materials Science Conference. 2006: McGill University, Montreal, QC, Canada.

[54] H. Tahiri, A.M. Samuel, F.H. Samuel, H.W. Doty and S. Valtierra, Mécanismes d'affinage des grains dans les alliages Al-Si en utilisant des alliages mères, in Int. Symposium on Aluminium : From Raw Materials to Applications, 45th annual Conf. of Metallurgists of CIM, C. 2006, Editor. 2006: Montreal, QC, Canada. pp. 863-880.

[55] K.B. Lee, H.S. Sim, S.Y. Cho Reaction products of Al-Mg/B4C composite fabricated by pressureless infiltration technique. Mater Sci Eng A, A302 (2001): pp. 227-234.

[56] K.E. Knipling, R.A. Karnesky, C.P. Lee, D.C. Dunand, D.N. Seidman, Precipitation evolution in Al-0.1Sc, Al-0.1Zr and Al-0.1Sc-0.1Zr (at. %) alloys during isochronal aging. Acta Mater, 58(2010), pp.5184-5195.

[57] K.E. Knipling, D.C. Dunand, D.N. Seidman, Criteria for developing castable, creep resistant aluminum-based alloys - A review. Z. Metallkunde, 97(2006):pp.246-265.

[58] K.E. Knipling , D.N. Seidman , D.C. Dunand, Ambient- and high-temperature Mechanical properties of isochronally aged Al-0.06Sc, Al-0.06Zr and Al-0.06Sc-0.06Zr (at.%) alloys. Acta Mater, 59 (2011); pp. 943-954.

[59] C.B. Fuller, D.N. Seidman, D.C. Dunand Mechanical properties of Al (Sc, Zr) alloys at ambient and elevated temperatures. Acta Mater, 51(2003):pp. 4803-4814.

[60] A.G.T. Miserez, Fracture and Toughening of High Volume Fraction Ceramic Particle Reinforced Metals. PhD Thesis, École Polytechnique Federale de Lausanne 2003.

[61] H. Zhang, M.W. Chen, K.T. Ramesh, J. Yed , J.M. Schoenung, S.C. Chin, Tensile behavior and dynamic failure of aluminum 6092/B4C composites. Mater. Sci. Eng A, A433(2006):pp.70-82.

[62] X. Kai, Y. Zhao, A. Wang, Hot deformation behavior of in situ nano ZrB2 reinforced 2024Al matrix composites. Compos Sci Technol, 116 (2015):pp. 1-8.

[63] M. Kouzeli and A. Mortensen A. Size dependent strengthening in particle reinforced aluminum. Acta Mater, 50 (2002): 39-51.

[64] M.C. Shankar, J. P. Ka, R. Shettya, Individual and combined effect of reinforcements on stir cast aluminum metal matrix composites-a review. Int J Curr Eng Technol, 3(2013): pp.922-934.

[65] X. Kai, Y. Zhao, A. Wang, Hot deformation behavior of in situ nano ZrB2 reinforced 2024Al matrix composites. Compos Sci Technol, 116(2015):pp. 1-8.

[66] M.E. Kassner, M-T Perez-Prado, Five-power-law creep in single phase metals and alloys. Prog Mater Sci, 45 (2000):pp. 1-102.

[67] M. Abo-Elkhier M.S. Soliman, Superplastic characteristics of fine-grained 7475 aluminum alloy. J Mater Eng Perform 15(2006): 76-80.

[68] M.J. McQueen M.E. Kassner Elevated temperature deformation: Hot working amplifies creep. Mater Sci Eng A, 58 (2005), pp. 410-411.

[69] Zhang H, Ramesh KT and Chin ESC. High strain rate response of aluminum 6092/B4C composites. Mater Sci Eng A, A384 (2004): 26-34.

[70] T.M. Lilo, Enhancing ductility of Al6061-10 wt.% B4C through equal-channel angular extrusion processing. Mater Sci Eng A, A410 (2005): pp.43-446.

[71] F.A. Mohamed, Correlation between creep behavior in Al-based solid solution alloys and powder metallurgy Al alloys, Mater. Sci. Eng. A 245 (1998) 242-256.

[72] E. Evangelista, S. Spigarelli, Constitutive equations for creep and plasticity of aluminum alloys produced by powder metallurgy and aluminum-based metal matrix composites, Metall. Mater. Trans. A 33A (2002) 373-381.

[73] S. Spigarelli, E. Evangelista, S. Cucchieri, Analysis of the creep response of an Al–17Si–4Cu–0.55Mg alloy, Mater. Sci. Eng. A 387-389 (2004) 702-705.

[74] F.A. Mohamed, K.T. Park, E.J. Lavernia, Creep Behavior of Discontinuous SiC-Al Composites, Mater. Sci. Eng. A 150 (1992) 21-35.

[75] R. Fernandez, G. Gonzalez-Doncel, Creep behavior of ingot and powder metallurgy 6061Al, J. Alloy Compd. 440 (2007) 158-167.

[76] K.T. Park, F.A. Mohamed, Creep strengthening in a discontinuous SiC-Al composite, Metall. Mater. Trans. A 26 (1995) 3119-3129.

[77] S. Spigarelli, E. Evangelista, H.J. McQueen, Study of hot workability of a heat treated AA6082 aluminum alloy, Scr. Mater. 49 (2003) 179-183.

[78] E.A. El-Danaf, A.A. Almajid, M.S. Soliman, High-temperature deformation and ductility of a modified 5083 Al alloy, J. Mater. Eng. Perform. 17 (2008) 572-579.

[79] E.A. El-Danaf, A.A. Almajid, M.S. Soliman, Hot deformation of

AA6082-T4 aluminum alloy, J. Mater. Sci. 43 (2008) 6324-6330.

[80] E.A. El-Danaf, M.S. Soliman, A.A. Almajid, Effect of solution heat treatment on the hot workability of Al-Mg-Si Alloy, Mater. Manuf. Process. 24 (2009) 637-643.

[81] S. Spigarelli, C. Paoletti, A new model for the description of creep behavior of aluminum-based composites reinforced with nanosized particles, Compos. Part A:Appl. Sci. Manuf. 112 (2018) 346-355.